Integrating Carbon Nanotube Forests into Polysilicon MEMS: Growth Kinetics, Mechanisms, and Adhesion

Stephen M. Ubnoske,[1*] Erich J. Radauscher,[2] Eric R. Meshot,[3] Brian R. Stoner,[4] Charles B. Parker,[2] and Jeffrey T. Glass[2]

[1]*Department of Mechanical Engineering and Materials Science, Duke University, Durham, NC 27708, USA*
[2]*Department of Electrical and Computer Engineering, Duke University, Durham, NC 27708, USA*
[3]*Physical and Life Sciences Directorate, Lawrence Livermore National Laboratory, Livermore, CA 94551, USA*
[4]*Research Triangle Institute (RTI) International, Durham, NC 27709, USA*

Abstract

The growth of carbon nanotubes (CNTs) on polycrystalline silicon substrates was studied to improve the design of CNT field emission sources for microelectromechanical systems (MEMS) applications and vacuum microelectronic devices (VMDs). Microwave plasma-enhanced chemical vapor deposition (PECVD) was used for CNT growth, resulting in CNTs that incorporate the catalyst particle at their base. The kinetics of CNT growth on polysilicon were compared to growth on Si (100) using the model of Deal and Grove, finding activation energies of 1.61 and 1.54 eV for the nucleation phase of growth and 1.90 and 3.69 eV for the diffusion-limited phase on Si (100) and polysilicon, respectively. Diffusivity values for growth on polysilicon were notably lower than the corresponding values on Si (100) and the growth process became diffusion-limited earlier. Evidence favors a surface diffusion growth mechanism involving diffusion of carbon precursor species along the length of the CNT forest to the catalyst at the base. Explanations for the differences in activation energies and diffusivities were elucidated by SEM analysis of the catalyst nanoparticle arrays and through wide-angle X-ray scattering (WAXS) of CNT forests. Finally, methods are presented to improve adhesion of CNT films during operation as field emitters, resulting in a 2.5x improvement.

1. Introduction

Vacuum microelectronic devices (VMDs) and sensors[1-6] present an attractive alternative to solid-state technology in applications where solid-state devices are unreliable or do not provide adequate performance. Situations that require high frequency and high power device performance, or operation in harsh environments such as high temperature or radiation, are ideal for vacuum microelectronics. While charges flowing through semiconducting channels tend to scatter, resulting in a loss of power and signal quality, electrons in a vacuum tube are unaffected by scattering loss[6]. Despite the performance advantages in certain applications, the use of vacuum electronics has been limited due to inadequate development of a suitable cathode that can be integrated into the common vacuum microelectromechanical systems (MEMS) platform. MEMS devices are fabricated by silicon-based microfabrication techniques[7], are constructed almost entirely from polycrystalline silicon (polysilicon or poly-Si) to achieve conductive structures and layered deposition, and can be micromachined into desired architectures. MEMS; a technology presently used as a platform for many types of navigation, automotive, and consumer microelectronic devices; offers a versatile and reliable microscale platform that can allow for integration of a large number of vacuum circuit elements on a single substrate.

Carbon nanotube (CNT) cold cathode field emitters have been shown to be excellent candidates for integration with MEMS[8-10] owing to their outstanding electrical and mechanical properties, allowing for the design and fabrication of complex and innovative integrated VMDs. To date, however, the factors involved with integrating CNTs as field emitters, specifically *in situ* growth of CNTs on polysilicon substrates,

have not been well studied. A scalable and reliable technology requires precise control over all components and conjoined materials. For CNT field emitters, precise control of the distance between the cathode and extraction electrode is critical to controlling power requirements and to avoid electrode shorting and device failure. Understanding CNT growth mechanisms, kinetics, and adhesion on MEMS substrate materials will enable seamless integration of CNT technology with existing standard MEMS processing techniques. CNT diameter, forest density, and length all influence field emission characteristics. Here, the focus will be on CNT growth kinetics as a means to developing fine control over these parameters.

While no studies have been performed on the kinetics and mechanisms of CNT growth on polysilicon, significant research has been performed studying growth kinetics and mechanisms for CNTs grown on single-crystal silicon by both thermal chemical vapor deposition (CVD) and plasma-enhanced chemical vapor deposition (PECVD). In early experiments by Baker *et al.*[11] on thermal growth of carbon nanofibers with catalyst particles fixed at the tips (tip-growth mode), bulk carbon diffusion through the catalyst was identified as the rate-limiting step due to the similarity of the growth activation energy with carbon diffusion. Similarly, Chhowalla *et al.*[12] reported a bulk-diffusion-limited growth process in tip-growth by PECVD, finding an activation energy of 1.4 eV and a growth rate that varied inversely with catalyst nanoparticle diameter[13]. Several other groups have reported activation energies in the range of 1.3 – 1.6 eV[14-16] and others have found the energy barrier to CNT growth closer to 2.2 – 2.4 eV[17-19]. Conversely, in the low-temperature regime (T = 150 – 500 °C), Hofmann *et al.*[20] reported a very low activation energy of 0.25 eV for tip-mode PECVD growth,

attributing the low value to surface diffusion of plasma-dissociated precursors across the catalyst particle. As such, bulk diffusion through the catalyst is not required for successful CNT growth. While most growth trends are nearly linear, especially for tip-mode thermal CVD deposition techniques, parabolic growth trends have been observed as well by several groups[21-24] in thermal CVD. This effect was attributed to gas phase diffusion-limited deposition. Wirth *et al.* found a pressure dependence of $p^{0.6}$ and activation energy of <1 eV for tip-growth thermal CVD[25], attributing observations to both dissociation of acetylene on the catalyst surface and a rate-limiting step of diffusion in the catalyst. Surface-diffusion-based growth mechanisms involving carbon precursor species traveling along the length of growing CNT forests have been described theoretically by Louchev *et al.*[26, 27]. In addition to a lack of literature addressing CNT growth kinetics on polysilicon substrates, there is little work studying higher temperature (800 – 900 °C) PECVD base-growth kinetics and mechanisms. Furthermore, there is no experimental work performed considering a mechanism involving a rate-limiting step of surface diffusion along the length of the growing CNT forest to the catalyst.

Despite significant efforts to understand CNT growth kinetics on single-crystal Si, little is known about growth on poly-Si substrates. Therefore, base-mode growth of CNTs by PECVD was studied on Si (100) and polysilicon substrates, fabricated identically to those fabricated in the industry-standard Polysilicon Multi-User MEMS Process, or PolyMUMPs, with the goal of modeling the same type of growth that occurs on MEMS devices. A parabolic growth trend was observed between CNT forest height and deposition time, separate activation energies corresponding to different phases of growth, and present evidence in favor of a growth mechanism dominated by surface

diffusion of carbon precursor along the outer surface of the CNTs, along the length to the catalyst fixed at the base of the CNT. Data is then presented to explain the causes of growth differences between CNTs deposited on Si (100) and CNTs deposited on poly-Si. Finally, thin film interlayers were engineered between the catalyst and the polysilicon substrate to improve the adhesion of CNT field emitters to the substrate.

2. Experimental

2.1. *Substrate Preparation*

The single-crystal silicon substrates used for the growth of CNTs in this study were N-type conductive (100) silicon. The polycrystalline silicon wafers were likewise fabricated at RTI International using a similar process to standard PolyMUMPs to replicate the substrate conditions for CNT growth on a MEMS device. A 1 μm thick polysilicon film was deposited on 500 μm thick N-type (100) silicon wafers via low-pressure CVD (LPCVD) followed by a 200 nm thick sacrificial layer of phosphosilicate glass (PSG) to serve as a phosphorus dopant source. The wafer was then annealed at 1050 °C for 1 hour in argon to n-dope the polysilicon as well as release stress in the polysilicon film formed during the LPCVD process. Next, the substrates were cleaned in a buffered oxide etch (BOE), rinsed with DI water, and dried with N_2 gas. All CNT growth substrates were coated with an iron catalyst layer 5 nm in thickness at RTI International using a CHA electron beam evaporation system.

Improvements in CNT adhesion to polysilicon substrates were made possible through the use of 2.5 nm thick metallic layers introduced between the polysilicon substrates (prepared as described above) and the thin film CNT catalyst. It has also been

shown[28-30] that these interlayers can result in better control of the final CNT film morphology by reducing catalyst diffusion into the poly-Si substrate during growth, but this was not directly investigated in this study. In order to compare the adhesion between CNT films with and without a metallic interlayer, samples of identical dimensions were fabricated for each of the interlayers, as well as a control sample that contained no interlayer. A dicing saw was used to precisely define 6.25 mm^2 substrates. Next, a brief BOE rinse was performed to remove any residue and then the substrate was loaded into the CHA electron beam evaporation system to deposit the refractory metal layers and iron catalyst.

2.2. *Carbon Nanotube Growth*

Microwave PECVD was employed for the growth of CNT forests on each type of substrate, which has been described in detail in previous publications [31-36]. In brief, the process occurs during two steps: heat up and growth. The heat up step involves raising the substrates to the desired deposition temperature, which is regulated by a thermocouple located directly under the quartz sample stage, followed by igniting and tuning a reducing plasma. The plasma is struck under a 100 sccm flow of NH_3 at the base reactor pressure (33 mTorr), and tuned to approximately 2.1 kW microwave power as the pressure in the reactor rises to 21 Torr. During this initial temperature and plasma ramp, the iron film dewets into catalyst nanoparticles. Following heat up, CH_4 is introduced as the carbon-containing precursor at a 150 sccm flow rate and the NH_3 flow is decreased to 50 sccm.

CNTs were grown for different time intervals (1, 2, 3, 4, and 5 minutes) at temperatures of 825, 850, and 875 °C on both Si (100) and polysilicon for the purpose of

identifying activation energies associated with different stages of growth. An extended range of deposition times was performed on each substrate at 850 °C in order to identify the diffusivity values of carbon feedstock through the growing CNT film. All CNTs possessed bamboo-type inner walls, as seen in Figure 1, and grew by base growth. The CNTs grown on polysilicon substrates frequently display a region of lower density, smaller diameter CNTs that extend past the tips of the bulk CNT film (Figure 1 (b)).

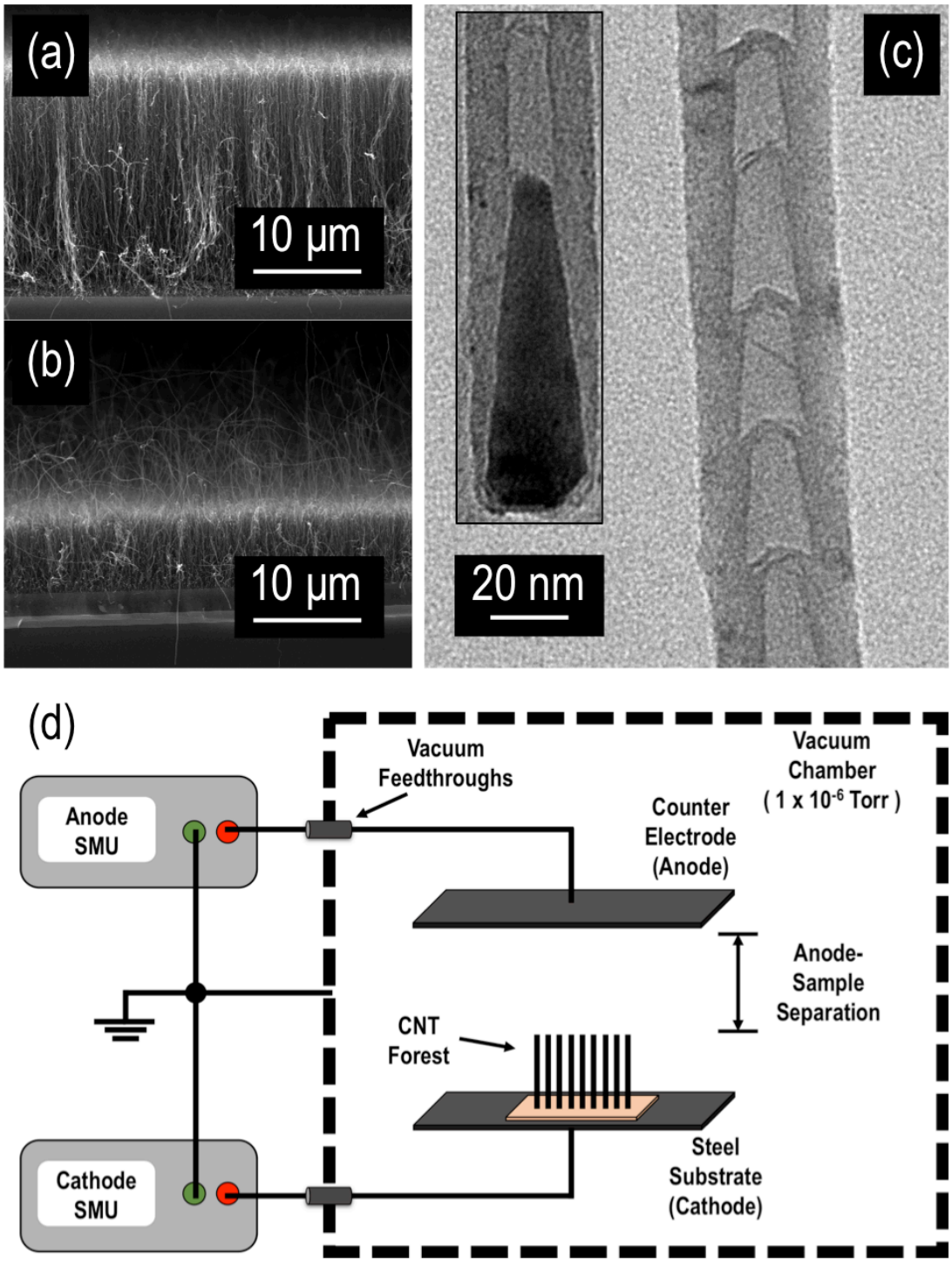

Figure 1: Morphology of CNTs simultaneously grown on a) Si (100) and b) polysilicon imaged by SEM. c) TEM micrograph of a CNT with bamboo-type inner walls, with inset depicting a catalyst iron nanoparticle embedded within the CNT base. d) Schematic of field emission test chamber (SMU: source measure unit).

2.3. *Characterization Techniques*

Scanning electron microscopy was performed with a FEI XL30 SEM-FEG microscope to measure the CNT film thickness and a FEI Tecnai G^2 Twin instrument was used to collect transmission electron microscopy images. Raman spectra were measured using a Horiba Jobin Yvon LabRam ARAMIS Raman microscope with a 633 nm HeNe laser. Synchrotron X-ray scattering measurements were performed at beamline 7.3.3 at the Advanced Light Source using a beam energy of 10 keV and a Mo/B_4C monochromator with the purpose of determining the extent of nanotube alignment. Alignment was quantified from the anisotropy of WAXS patterns using Herman's orientation factor (*f*)[37] which has a value between 0 and 1. Values closer to 1 indicate a higher degree of alignment.

2.4. *Adhesion Testing*

Adhesion of the CNT emitters to the substrate was examined using the standard American Society for Testing and Materials (ASTM) test methods for measuring adhesion of thin films[38], which assesses the adhesion of films to substrates by applying and removing pressure-sensitive tape over the film (3M Magic Tape 810D). This procedure was combined with spectrophotometer measurements performed after each tape test in order to measure the reflectance from the underlying sample. More than ten samples from each interlayer set were tested with 50-60 spectrophotometer measurements performed on each sample for statistical relevance. The reflectance correlated directly to the CNT density remaining on the sample after each adhesion test, which provided quantitative measurements of the degree of adhesion of the CNT film to the substrate. Each sample was mounted onto a custom 3D-printed sample holder that was designed to

be compatible with a Shimadzu UV-3600 UV-Vis-NIR Spectrophotometer. The instrument was operated in reflectance mode, scanning wavelengths between 200 and 700 nm. After the baseline measurements, the sample holder was removed from the instrument and the first tape test was performed. Constant pressure was applied using fixed weights that were moved uniformly across the film surface and tape removal speed was carefully monitored. However, it has been shown[39] that variability in the speed at which the tape is removed, as well as the variability in applied pressure, do not strongly impact adhesion evaluation. As a subject for future work, direct measurement of the peeling force may be added to this analysis for a more robust adhesion data set. Nonetheless, due to the consistently applied pressure to the tape and the consistent rate of removal, this method allows for semi-quantitative comparison of the adhesion of the CNT film with different metal interlayers. After the tape was removed, the sample was loaded back into the spectrophotometer for another set of reflectance measurements. This process was repeated until the reflectance measurements saturated, indicating that all possible CNTs were removed.

3. Results and Discussion

3.1. *CNT Growth Kinetics and Activation Energies*

A model of the growth kinetics was performed for each substrate in order to understand the differences between CNT growth on crystalline silicon substrates using PECVD and the corresponding growth on a polysilicon substrate. A model based on Fick's first law for a thin membrane[40] was used in a similar way to the Deal and Grove model of thermal oxidation of silicon[23, 24, 41]. A more detailed description of the

model may be found in the Supporting Information. In short, the flux of carbon species through the boundary consisting of the tip of the CNT forest is given by Fick's first law and the diffusion constant for carbon through this boundary layer as well as the thickness of the boundary are assumed constant in space and time. The steady-state assumption is also in effect, whereby the flux of carbon species impinging upon the growing CNT array is assumed equal to the flux of carbon species through the CNT array and also equal to the flux through the catalyst particle[42]. If N is the number of carbon species that diffuse into the iron catalyst and are subsequently incorporated into the CNT film and F is the overall flux, the growth rate of the forest may be expressed as

$$dL/dt = F/N \tag{1}$$

The general solution to this expression takes the form

$$B(t_{gr}) = AL + L^2 \tag{2}$$

where A and B may be expressed in terms of the diffusivity D, which is proportional to $\exp\left(-E_a / K_B T\right)$, k_B is Boltzmann's constant, T is the growth temperature, and t_{gr} is the growth time[41, 42]. For short growth times, hereafter referred to as the linear region, equation (2) may be approximated as $B(t_{gr}) \approx AL$, and thus the linear rate constant is B/A. For longer growth times, equation (2) may be approximated as $B(t_{gr}) \approx L^2$ which will be referred to as the parabolic growth regime. The parabolic region corresponds to deposition times when the growing CNT forest presents a barrier to the diffusion of carbon precursors to the catalyst at the substrate surface, and the linear region corresponds to all growth times prior. Saturation of the catalyst particle with carbon as well as nucleation of CNTs occur during the linear phase of growth. From the relationship between the linear rate constant and the activation energy associated with the

physical process that occurs during this period (*i.e.*, carbon diffusion into the catalyst and nucleation of CNTs), the activation energy may be calculated via the slope of the corresponding Arrhenius plot. Likewise, the activation energy corresponding to the physical process occurring during the parabolic region (*i.e.*, the diffusion of carbon feedstock from the gas phase to the catalyst through the growing nanotube forest) may be determined in the same way using the parabolic rate constant *B*[42]. The termination growth regime, existing for growth times exceeding the time steps considered for the parabolic region, is not discussed here, although reports of CNT growth termination mechanisms may be found in the literature[43-46].

As discussed in the Experimental Section, to determine the activation energies for each phase of growth, growth temperatures of 825, 850, and 875 °C were used for deposition times of 1, 2, 3, 4, and 5 minutes. As such, each point in Figure 2 represents of five growth data points. During each growth experiment, Si (100) and polysilicon substrates were loaded simultaneously in the PECVD reactor, and the film thickness for each was measured by SEM. Figure 2 is the Arrhenius plot displaying the natural logarithm of both the linear and parabolic rate constants as a function of inverse temperature. The slope (*m*) of the Arrhenius curve is related to activation energy by $E_a = -K_B m$. The results of this analysis indicate activation energies during nucleation corresponding to diffusion of carbon feedstock into the catalyst of $E_{a,lin}^{Si}$ = 1.61 eV on the Si (100) substrates, and $E_{a,lin}^{poly-Si}$ = 1.54 eV on polysilicon substrates. These values closely match the literature values for bulk diffusion of carbon into γ-Fe, which have been reported in the range of 1.54-1.6 eV[47]. While γ-Fe typically does not form below a temperature of 912 °C[48], the existence of residual carbon in the PECVD reaction

chamber could allow for the formation of γ-Fe rather than α-Fe or a mixed phase. On the other hand, activation energies from the parabolic growth regime were found to be $E_{a,para}^{Si}$ = 1.90 eV and $E_{a,para}^{poly-Si}$ = 3.69 eV for CNTs grown on Si (100) and polysilicon substrates respectively.

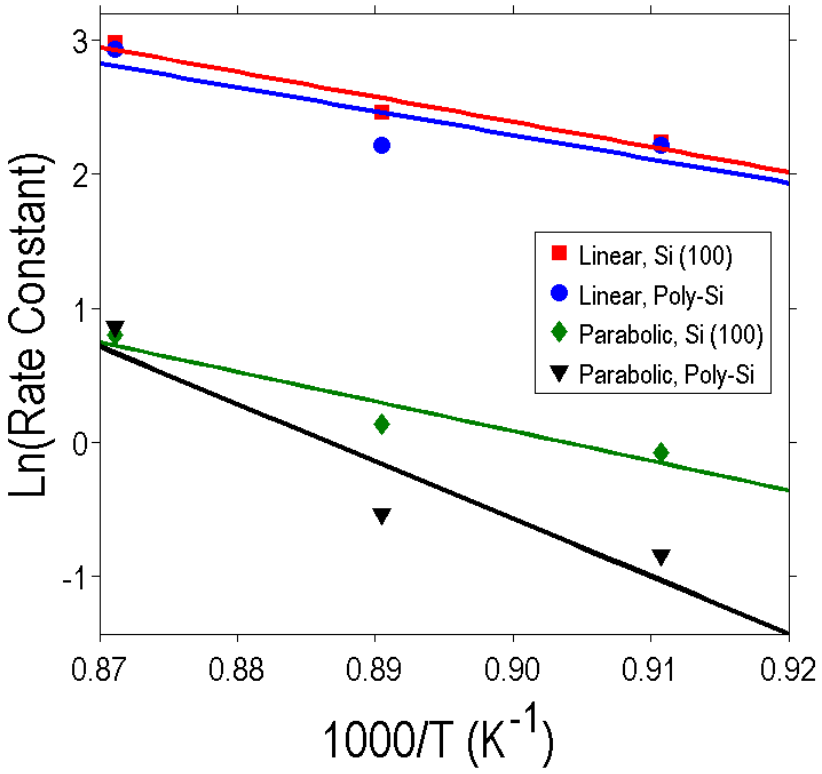

Figure 2: Arrhenius plot used to determine activation energies corresponding to the linear and parabolic regions of CNT growth. The slope of the linear region for both substrates is quite similar and corresponds to bulk diffusion of carbon precursor into the γ-Fe catalyst nanoparticles. The slope in the parabolic region differs between CNTs on Si (100) and polysilicon, leading to different activation energies for the diffusion-limited phase of growth. Each data point is a composite of five growth data points.

To understand the physical processes responsible for the increased energy barrier during CNT growth compared with bulk diffusion occurring during nucleation, as well as to understand parabolic activation energy differences between growth on each substrate, the theory of diffusion developed by Deal and Grove[41] was again employed. The overall growth rate expression used to fit growth rate data is

$$R(t) = 0.5A\left(\sqrt{1+\frac{4B(t_{gr})}{A^2}}-1\right) \qquad (3)$$

where R is the height of the CNT forest, t_{gr} is the growth time, and A and B are composite terms previously discussed, defined as

$$A = 2D/k \quad , \quad B = 2Dn_0/n_s \tag{4}$$

D is the diffusivity, k is the effective rate constant for the conversion of feedstock into nanotubes, n_0 is the concentration of feedstock at the tips of the CNTs as estimated by the ideal gas law[49], and n_s is the density of the deposited nanotubes (0.02 g cm^{-3})[23].

A more robust data set was needed to effectively fit Equation (3), and thus another growth series was performed at 850 °C with growth times of 20, 30, 40, 50, 60, 120, 240, and 480 s. Equation (3) was fit to the above set of data treating A and B as constants to determine through the fit. The Levenberg-Marquardt nonlinear least squares algorithm was used to calculate values of A and B, which were subsequently used to extract diffusivity values (Figure 3). The diffusivity values calculated by this method were 3.5 x 10^{-4} cm^2/s and 7.9 x 10^{-5} cm^2/s for CNT growth on Si (100) and polysilicon substrates, respectively.

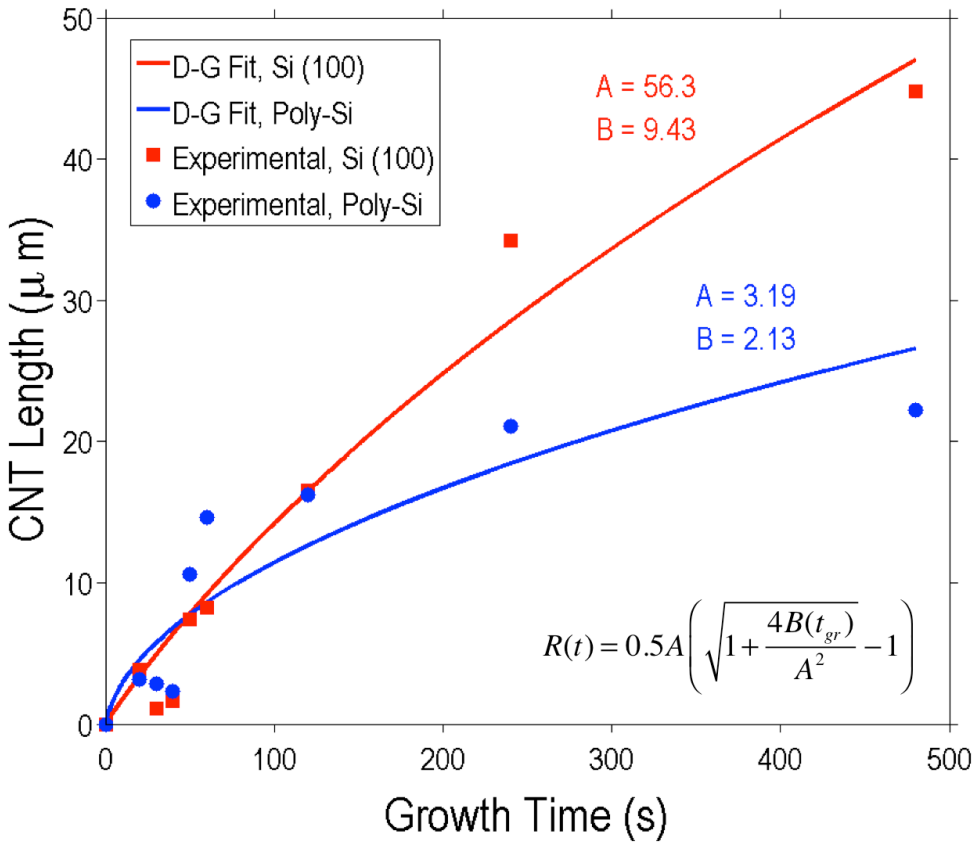

Figure 3: CNT forest height kinetics at 850 °C. The solid curves correspond to the fit to the Deal and Grove expression, with A and B values listed.

To determine the degree to which the growth process is diffusion-limited, a quantity referred to as the diffusion-limiting factor α was calculated in a similar fashion to Puretzky *et al*[23]. The time-dependent term found under the radical in Equation (3) clearly plays a crucial role in the curvature of the length vs. deposition time curve for a CNT growth reaction, and is defined as

$$\alpha(t_{gr}) = 4Bt_{gr}/A^2 = 2n_0k^2t_{gr}/Dn_s \tag{5}$$

Based on the fit of the Deal and Grove expression, the corresponding values of the diffusion-limiting factor as a function of growth time are $\alpha_{Si} = 0.012t_{gr}$ and $\alpha_{poly-Si} = 0.834t_{gr}$ for growth at 850 °C. In order for the process to be considered

diffusion-limited, $\alpha >> 1$ [23]. Therefore, it is clear that growth of CNTs on polysilicon becomes diffusion-limited about 10 times faster compared with CNTs grown on Si (100), resulting in a CNT growth rate reduction earlier in the growth process on poly-Si compared to Si (100).

3.2. *Diffusion Mechanisms*

Considering the above description of CNT growth kinetics on Si (100) and polysilicon substrates, three closely related issues have arisen. First, the activation energy for the parabolic region of growth is higher than the bulk activation energy calculated for the linear region associated with nucleation. Furthermore, the activation energy found for the parabolic region of growth on polysilicon is significantly larger than the equivalent energy barrier for growth on Si (100). Finally, the diffusivity of carbon precursors through the growing CNT forest on polysilicon is significantly lower than the diffusivity for growth on Si (100). To understand the factors giving rise to these observations, the physical diffusion mechanisms of the growth process must be considered under the PECVD growth conditions.

The diffusion mechanisms most relevant to a porous thin film system are Knudsen diffusion and surface diffusion. Knudsen diffusion involves the collision of gas molecules with pore walls as a means of gas transport through the pore, or the space between CNTs in the present case. Knudsen diffusion may occur in a system if the pore size is smaller than the mean free path of the gas molecules by a factor of ten or more[24, 50, 51]. Knudsen diffusion is commonly cited as the governing diffusion mechanism for CNT growth by thermal CVD[23, 24]. An alternative mechanism is surface diffusion of carbon molecules or radicals along the surface of growing CNTs as a means of transport

from the gas phase to the catalyst particle at the substrate surface. This mechanism has been theorized by Louchev *et al.*[26, 27], and may be a more likely governing diffusion mechanism when the carbon precursors are in the form of reactive radicals. While the conditions are met for Knudsen diffusion in the current system, evidence is presented below in favor of surface diffusion along the CNT length being the primary transport mechanism for this PECVD process. Specifically, a trend of decreasing CNT length with increasing process temperature, defect density for CNTs grown on each substrate, the growth mechanism for a graphene-CNT hybrid material, and the existence of bamboo-type inner CNT walls will be discussed in the context of a surface diffusion mechanism, offering supporting evidence that the growth process is controlled by this mechanism.

A conclusive way to determine the diffusion mechanism is to determine the temperature dependence of the diffusivity of the system. By calculating diffusivity at a number of temperatures and examining whether these values correspond to a $T^{1/2}$ dependence or a exp(*-1/T*) dependence, it is possible to determine whether the governing mechanism is Knudsen diffusion or surface diffusion, respectively. As this analysis requires more data than is presently available, several pieces of supporting evidence are instead proposed in favor of the surface diffusion mechanism.

The first potential mechanism to consider is Knudsen diffusion. The Knudsen number, the figure of merit determining whether transport is governed by Knudsen diffusion, is the ratio of the pore size (r) to the mean free path of the carbon-containing precursor (λ_{MFP}). If this ratio is less than 0.1, Knudsen diffusion may occur[24, 50, 51]. Mean free path may be calculated as[52]

$$\lambda_{MFP} = RT / \sqrt{2}\pi d^2 N_A p \qquad (6)$$

where R is the ideal gas constant, T is the temperature, d is the molecular diameter, N_A is Avogadro's number, and p is the chamber pressure. Using methane as the carbon-carrying species and the growth parameters enumerated in the Experimental Section, $\lambda_{MFP} \approx 7.8$ μm. Since the inter-CNT pore size is on the order of tens of nanometers, the above ratio is much less than 0.1. Therefore, it is possible that some Knudsen diffusion may occur during growth. It seems unlikely, however, that this is the primary diffusion mechanism, as most carbon-containing species exist in the form of reactive radicals due to the presence of the plasma. Additionally, the CNTs possess a high defect density due to ion bombardment, which may serve as adhesion sites for reactive radicals and hinder Knudsen diffusion.

There are several pieces of supporting evidence that favor surface diffusion along the length of the CNTs as the primary diffusion-limiting mechanism during steady-state growth. In the case of iron-catalyzed growth in this PECVD reactor, the growth proceeds from the iron catalyst nanoparticles, which remain anchored at the substrate-nanotube interface. A growth mechanism dominated by surface diffusion must allow for diffusion of carbon species from the gas-nanotube interface to the catalyst particle at the substrate surface, so surface diffusion must occur along the length of the CNTs.

Across a wider temperature range (700 – 900 °C), a general inverse relationship between CNT forest height and growth temperature on MEMS devices was observed (Figure 4). These growth experiments on polysilicon MEMS devices were performed under identical growth conditions but varying the process temperature. This trend is also reflected in the results of several other mechanistic studies[12, 27, 53, 54], and was initially attributed to diffusion of the catalyst into the polysilicon substrate. However, it

is unlikely that a significant amount of iron silicide exists in the catalyst nanoparticles, at least during the linear phase of growth, due to the earlier conclusion that the nanoparticles are austenite, which does not form readily if a significant amount of silicon has become incorporated into the nanoparticle[55].

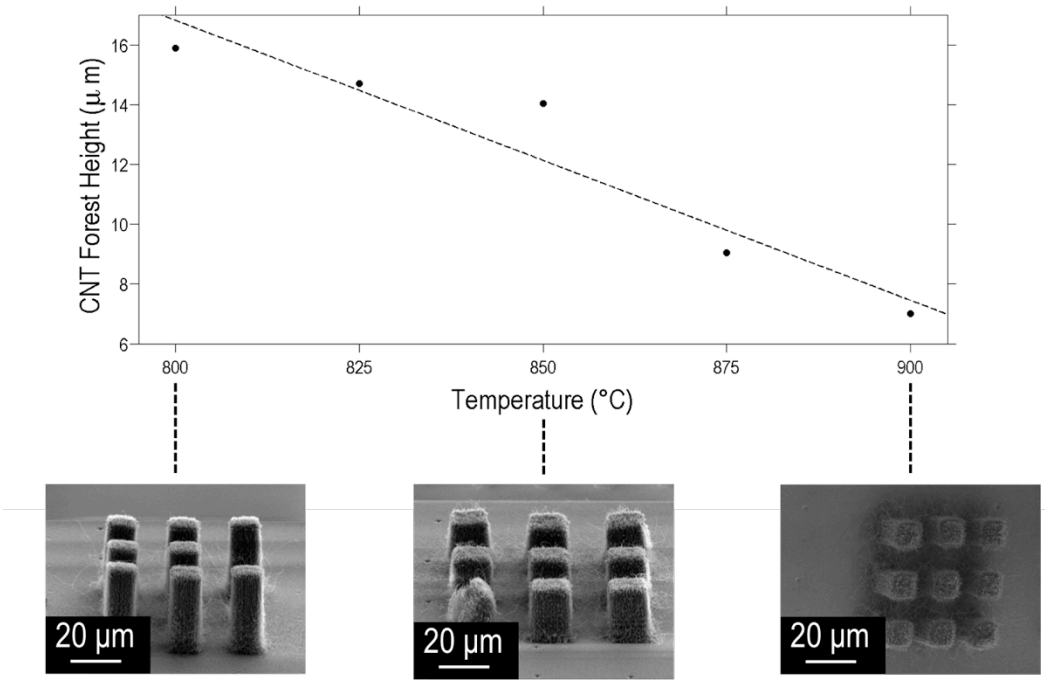

Figure 4: CNT forest height as a function of growth temperature on polysilicon MEMS devices. All CNT forests were grown for 150 s.

The trend of decreasing CNT length as a function of increasing temperature can be explained if the majority of the diffusion of carbon species from the gas phase to the catalyst particle occurs by the surface diffusion mechanism along the CNT sidewalls. The average distance that a carbon species may travel along the length of a CNT before coming to rest is given by[27]

$$\lambda_{SD} = a_0 \exp\left[\left(E_{ads} - E_{SD}\right)/2K_B T\right] \tag{7}$$

where a_0 is the distance between adsorption sites on the CNT surface, E_{ads} is the energy barrier to adsorption, and E_{SD} is the activation energy of surface diffusion along the

length of the CNT. Under these experimental conditions and using literature values to approximate the different energy barriers, λ_{SD} is on the order of tens of micrometers, and this characteristic length is reduced strongly with increasing temperature. Therefore, it is possible that the reduction in CNT length with increasing temperature on polysilicon MEMS devices is primarily due to the decrease in surface diffusion length.

In order to elucidate the surface diffusion mechanism as well as understand the large activation energy for the parabolic growth region on polysilicon substrates, Raman spectroscopy was used to measure the mean distance between defect sites on CNTs grown on each substrate. Through the Tuinstra-Koenig relationship[56], it is possible to calculate the mean crystallite size (L_a) of CNTs by studying the relative intensities of the *D* and *G* Raman bands. This expression was modified by Matthews *et al.* to take into account the wavelength of the incident laser[57]. As seen in Figure 5, there is a significant difference in L_a between CNTs grown on Si (100) and polysilicon, which were found to be 6.60 and 20.1 nm respectively. This difference in L_a may arise from the presence of smaller catalyst nanoparticles on poly-Si substrates, discussed below in Section 3.3, which could produce CNTs that are smaller in diameter and more crystalline. If it is assumed that L_a is a good approximation to a_0 in Equation (7), the distance between adsorption sites that act as a pathway to surface diffusion along the length of the CNTs is larger for CNTs grown on polysilicon. This may explain the large E_a for the parabolic region of growth on polysilicon (3.69 eV) compared to CNTs grown on Si (100) (1.90 eV), as the energy barrier for transport between adsorption sites should increase with increasing distance between adsorption sites. In addition, the parabolic

activation energy for CNTs grown on Si (100) is close to the reported value for carbon adsorption on CNT sidewalls[27, 58].

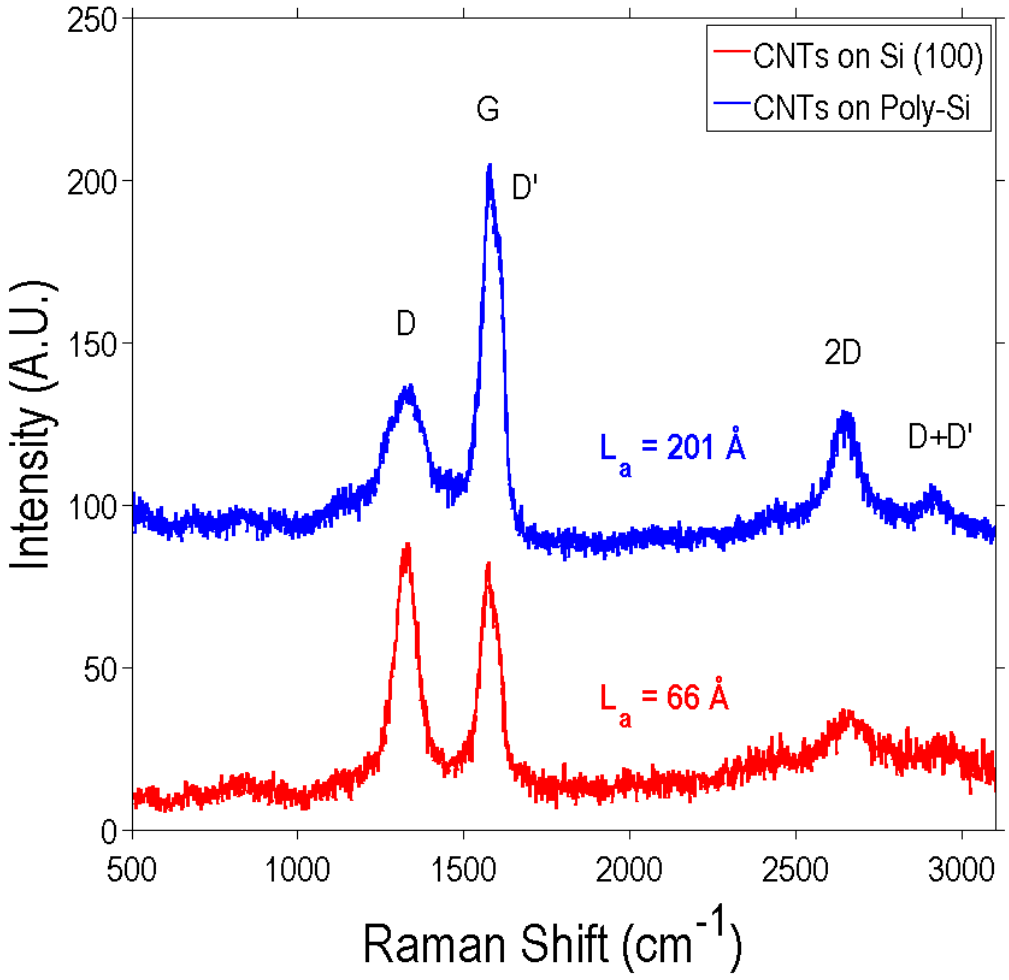

Figure 5: Raman spectra of CNTs grown on Si (100) and polysilicon substrates. The crystallite size is 66 Å for CNT on Si (100) and 201 Å for CNTs on polysilicon.

More support of surface diffusion as the primary diffusion mechanism in this system comes from the existence of a hybrid carbon nanostructure consisting of few-layered graphene covalently bonded to the sidewalls of CNTs referred to as graphenated carbon nanotubes (g-CNTs). As reported elsewhere[31-35, 59], this hybrid nanostructure (Figure 6) usually requires an elevated temperature (1050 °C) in order to form the leaves of few-layered graphene, referred to as "foliates." The growth mechanism of these

foliates has been proposed as either a stress-buckling mechanism[32] where varying growth rates between concentric nanotube walls causes buckling and fracture, allowing growth of the foliate at the fracture site, or an ion bombardment mechanism[33] where energetic ions from the plasma environment cause defects in the outer nanotube walls, allowing foliates to nucleate and grow. In either case, defect sites in the outer walls of the CNTs exist at high spatial frequency, which is also the pathway by which surface diffusion-driven growth occurs. However, at the elevated temperatures used to grow g-CNTs, growth typically terminates at about 10 μm, after which point growth of foliates begins[32, 33]. This lower terminal length is in agreement with a surface diffusion mechanism that limits the maximum forest length as temperature is increased. If the temperature during growth remains lower (850 °C), these g-CNT structures may also form, but only when the growth time is much longer[34]. These lower temperature g-CNTs also form foliates only after the termination length of the forest is reached, which is typically 40-50 μm at 850 °C.

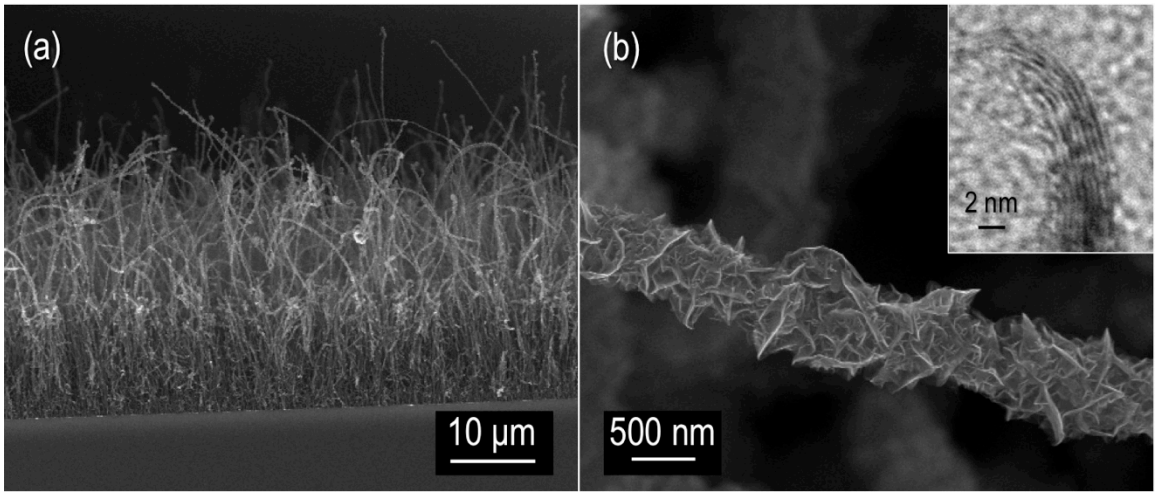

Figure 6: a) Plan view SEM micrograph of graphenated CNTs and b) higher magnification image of a g-CNT. Inset: TEM micrograph of a few-layered graphene foliate terminating in 3-5 graphene layers.

Temperature gradients within the growing CNT array also support a surface diffusion mechanism. There are two heat sources during the growth reaction: the substrate heater underneath the growth substrate and the plasma above the growing CNT array. The heat generated in the CNT film by ion- and reactive radical-bombardment from the plasma, powered by 2.1 kW of microwave power, should be higher than that of the substrate heater, so a thermal gradient exists in the downward direction away from the plasma. As a result, the CNT tips are the hottest regions of the film. After growth terminates due to the limitation in surface diffusion length, the tips continue to experience reactive carbon-containing radicals impinging upon them. As the tips are at a higher temperature than the lower regions of the CNTs due to the aforementioned thermal gradient as well as heat loss occurring from conductive losses along the length of the tube and convective loss from gas molecules in the region between CNTs (due to some limited Knudsen diffusion), the surface diffusion length is smallest for this region. As carbon species adsorb onto the CNT tips, surface diffusion may occur over a very small length scale, especially at higher growth temperatures, and nucleate foliates at the defect site where it comes to rest. In this way, surface diffusion seems the most likely mechanism in light of the evidence presented for this hybrid nanostructure.

Additionally, it has been observed that when the temperature is increased further (1100 °C or higher), CNTs or g-CNTs are no longer present in the resultant film. Instead, vertically oriented sheets of few-layered graphene are deposited on the substrate without any nanotube structure present[33]. As the CNTs grown by this PECVD reaction have bamboo-type inner CNT walls, it is possible that the surface diffusion length is even shorter for these conditions than the length of a single bamboo segment, preventing the

growth of nanotubes. Instead, carbon nanosheets are produced at temperatures exceeding 1100 °C[33].

As a final point supporting the surface diffusion mechanism, bamboo-type growth has been associated with a surface diffusion mechanism[26].

3.3. *Causes of Reduced Diffusivity for CNTs grown on Polysilicon*

Thus far, the kinetics of CNT growth on polysilicon has been discussed and compared to growth on Si (100), the physical interpretation of the associated activation energies has been examined, and diffusion mechanisms have been explored. Here, the reason why growth on polysilicon has lower diffusivity and becomes diffusion-limited earlier in the growth process compared with CNTs grown on Si (100) will be considered.

It is well known that the diameter of the catalyst nanoparticles is closely related to the diameter and growth rate of the resultant CNT [12, 60, 61]. Catalyst nanoparticle diameter and CNT diameter are directly proportional, and CNT diameter and CNT growth rate are inversely proportional. It is therefore important to examine the way in which the iron catalyst film dewets on poly-Si versus Si (100). Figure 7 shows SEM micrographs of catalyst nanoparticles forming on each substrate at 850 °C, prepared by terminating the CNT growth process before introduction of the carbon precursor, as well as the diameter distribution of these nanoparticle arrays. From Figure 7, it is clear that nanoparticles on polysilicon are less uniform. The highest frequency nanoparticle diameter is between 15 and 30 nm and the nanoparticles have a bimodal distribution. In contrast, the nanoparticles that form on Si (100) substrates possess more uniform diameters and are larger on average. Additionally, the nanoparticles that form on top of the grains on polysilicon substrates tend to be larger (60-70 nm) and smaller particles

aggregate near the grain boundaries. The lower mode in the bimodal distribution is attributed to particles formed around the grain boundaries, where the crystal facets are expected to vary. This is in agreement with literature[62], in which smaller particles form on the Si (111) crystal face (25-35 nm) and larger particles (55-65 nm) form on Si (100) due to differences in surface energy. While catalyst thickness and pretreatment time impact the resultant nanoparticle dimensions[63, 64], these parameters were very similar in the referenced study compared to the present experimental conditions.

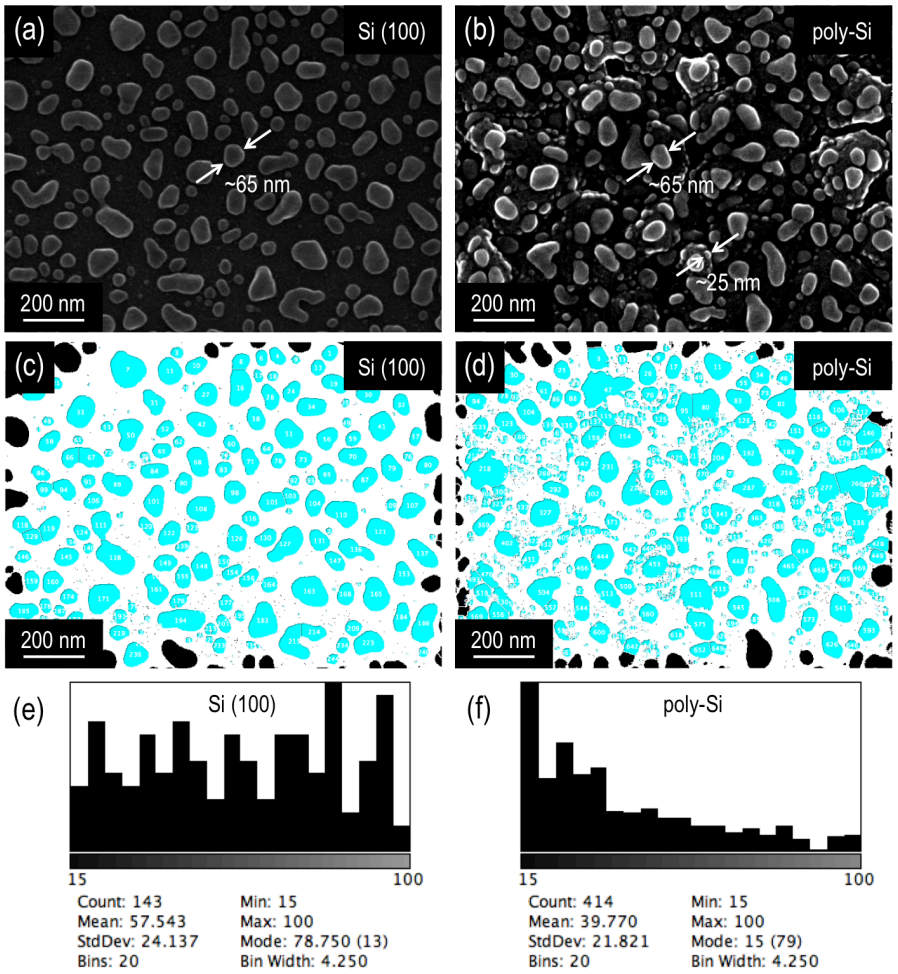

Figure 7: Catalyst nanoparticle arrays produced by dewetting at 850 °C in an ammonia plasma environment on a) Si(100) and b) polysilicon. (c-d) illustrate image processing performed in order to obtain the nanoparticle diameter distributions, found in (e-f). (e-f) display the distributions of Feret diameters, excluding particles found at the edge of the image.

As mentioned above, the catalyst nanoparticle diameter influences the resultant CNT diameter as well as growth rate. Since the nanoparticle diameters are dispersed across a wider range on polysilicon compared to Si (100) substrates, there is a corresponding dispersion of growth rate of the nanotubes catalyzed by these particles. Due to the close proximity of CNTs to one another during the growth process, van der Waals forces[65, 66] may cause neighboring CNTs with differing growth rates to collectively bend and become tortuous. Since the dispersion of nanoparticle diameters is higher for CNTs grown on polysilicon due to the variety of surface energies displayed by the various exposed crystal faces, the tortuosity of these films is expected to be higher. CNT films with a higher degree of tortuosity have a lower apparent film thickness for a given CNT length due to the compression of CNT length along the vertical direction[67]. Therefore, an increase in tortuosity leads to a reduction in apparent growth rate and a reduction in diffusivity, as is observed for CNT growth on polysilicon versus Si (100). This discrepancy would be eliminated if real CNT length were used for kinetics calculations rather than film thickness.

In order to measure the difference in tortuosity for CNTs grown on each substrate, wide-angle X-ray scattering (WAXS) measurements were taken to quantify the degree of alignment of each type of film. As discussed in the Experimental Section, the orientation factor (*f*) for typical aligned CNT films grown on Si (100) and polysilicon substrates was determined in order to corroborate the conclusions made from the nanoparticle analysis. The orientation parameter is calculated from anisotropy in the X-ray scattering pattern,

$$f = \frac{1}{2}\left(3\left\langle \cos^2 \phi \right\rangle - 1\right) \tag{8}$$

where

$$\left\langle \cos^2\phi \right\rangle = \frac{\int_0^{\pi/2} \left(I(\phi) \sin\phi \cos^2\phi \right) d\phi}{\int_0^{\pi/2} \left(I(\phi) \sin\phi \right) d\phi} \tag{9}$$

φ is the angle between the z-axis and the vertically-oriented CNT, while $I(\varphi)$ is the azimuthal intensity distribution collected at the q location of maximum intensity[37, 68], corresponding to the interlayer spacing of the graphitic sidewalls.

For CNTs grown on Si (100), $f_{Si} = 0.4$ and for CNTs grown on polysilicon, $f_{poly\text{-}Si} = 0.2$. From these values, it is clear that the CNTs grown on polysilicon have higher tortuosity compared with CNTs grown on Si (100) (Figure 8). This may also help to explain why the calculated diffusivity is markedly lower for growth on polysilicon and the parabolic activation energy is larger, as the effective growth rate disparity is reduced when taking tortuosity into account.

To elaborate on this idea, one may calculate the tortuosity-corrected CNT length via the Herman's orientation parameter as

$$\Delta l = \left(\frac{3}{2f+1} \right)^{1/2} \Delta z \,, \tag{10}$$

where Δl represents the effective film thickness accounting for tortuosity and Δz is the apparent film thickness as measured by SEM[35, 67, 69]. In the present case, WAXS data is available for a representative CNT film on Si (100) and poly-Si. Ideally, however, changes in tortuosity should be monitored at each growth time step or *in situ* (see Ref. [67] for *in situ* WAXS analysis of CNT growth). The calculations that follow are approximate, as a representative sample was used for each type of film for the calculation

of Herman's orientation parameter. Identically-prepared samples may exhibit minor differences in this value due to small, unintentional morphological variations.

Using the tortuosity-corrected values for CNT length and performing the same analysis found in Section 3.1, $E_{a,lin}^{Si}$, $E_{a,para}^{Si}$, and $E_{a,lin}^{poly-Si}$ remain unchanged within three significant figures and $E_{a,para}^{poly-Si}$ decreases slightly from 3.69 eV to 3.06 eV. The greater difference in the latter value stems from its steeper slope in the Arrhenius plot.

Applying the same tortuosity correction to the diffusivity calculation in Section 3.1, the diffusivity value for CNT growth increases on each substrate to 5.82 x 10^4 cm^2/s on Si (100) and 1.69 x 10^4 cm^2/s on poly-Si, as the effective growth rate is higher when taking CNT tortuosity into account. The ratios of diffusivity values on each substrate are $D_{850°C}^{Si} / D_{850°C}^{poly-Si} = 4.43$ and $D_{850°C}^{t,Si} / D_{850°C}^{t,poly-Si} = 3.44$ before and after correcting for CNT tortuosity, respectively. Thus the difference in diffusivity between CNT films grown on Si (100) and poly-Si is slightly reduced when taking tortuosity into account due to the higher degree of tortuosity of the CNT films grown on poly-Si. However, diffusivity remains significantly higher for films grown on Si (100). As a result, the evidence presented in Section 3.2 in favor of a surface diffusion-based CNT growth mechanism as well as the causes for reduced diffusivity of CNTs grown on poly-Si found in Section 3.3 remain valid. The tortuosity-corrected kinetics figures of merit are summarized in **Table 1**.

Table 1

Kinetics figures of merit for CNTs grown on Si (100) and poly-Si with and without correction for CNT tortuosity.

Substrate	$E_{a,lin}$ (eV)	$E_{a,para}$ (eV)	$E^t_{a,lin}$ (eV)	$E^t_{a,para}$ (eV)	$D_{850°C}$ (x10^4 cm^2/s)	$D^t_{850°C}$ (x10^4 cm^2/s)
Si (100)	1.61	1.90	1.61	1.90	3.49	5.82
Poly-Si	1.54	3.69	1.54	3.06	0.787	1.69

$E_{a,lin}$ is the activation energy in the linear region of growth, $E_{a,para}$ is the activation energy in the parabolic region of growth, and $D_{850°C}$ is the diffusivity of CNT growth at 850 °C. Superscript *t* denotes a tortuosity-corrected value.

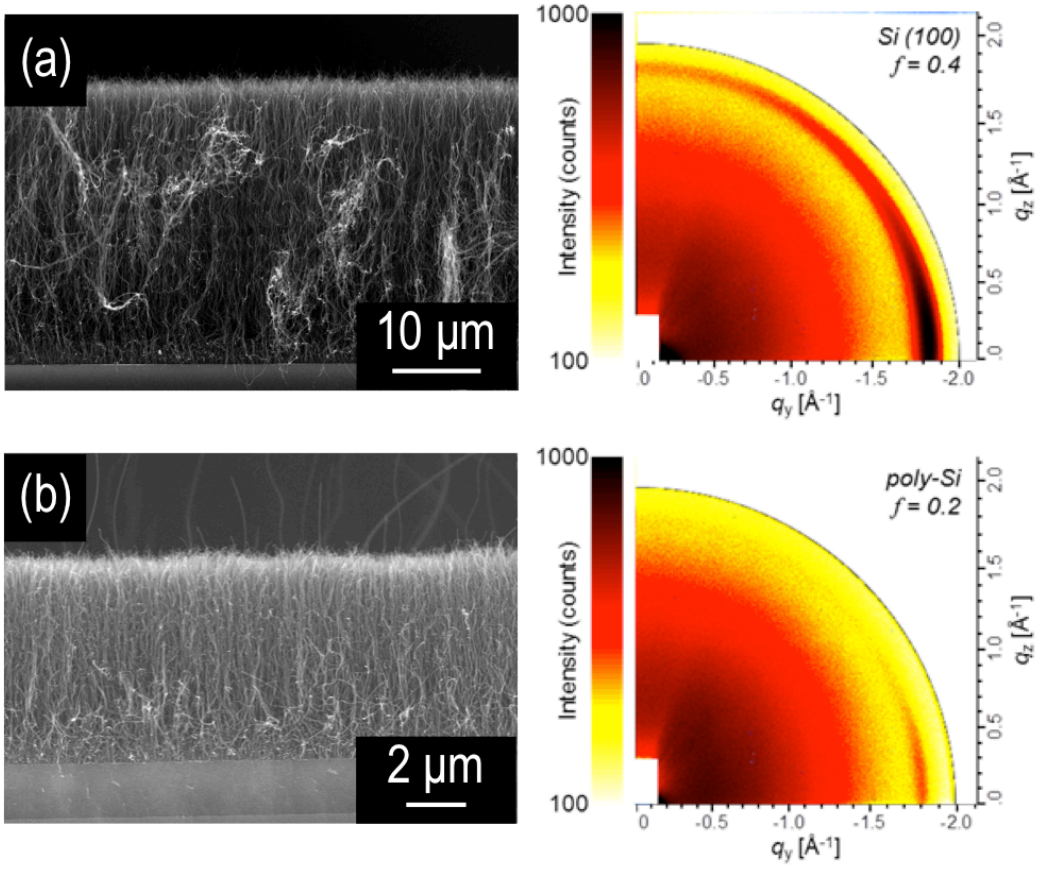

Figure 8: WAXS spectra of CNTs grown on (a) Si (100) and (b) poly-Si. The CNTs on poly-Si display a higher degree of tortuosity, with an orientation factor of approximately 0.2. The orientation factor of CNTs on Si (100) is approximately 0.4.

Other possibilities to consider to account for differences in CNT growth kinetics include the temperature-dependent nature of the gas atmosphere as well as the temperature dependence of the catalyst nanoparticle array. As this is a plasma-enhanced CVD process, the gas atmosphere is dominated by the microwave plasma, whose

temperature is governed by the microwave energy input. In addition, the range of temperature setpoints for the substrate heater was narrow, only spanning 825-875 °C. Therefore, differences in precursor chemistry are expected to be negligible for these experiments.

Examining the diameters of the nanoparticles within the temperature range of 825-875 °C in the same way as illustrated in Figure 7, there was a difference of 6% on poly-Si substrates and <1% on Si substrates. These small diameter differences are within the range of typical variations between PECVD experiments performed at the same temperature. In addition, while catalyst nanoparticles possess some mobility during the heat up stage of the reaction, nanoparticle mobility ceases to play a role once CNTs have nucleated and encapsulated the nanoparticles (see Figure 1 (c)) as the growth of CNTs anchors the nanoparticles on the substrate. Therefore, due to the narrow temperature window of this study, variations in the catalyst nanoparticles between growth experiments are small and unlikely to affect the outcomes of the kinetics analysis. Finally, all growth experiments were performed with sufficiently small growth times and a sufficiently narrow temperature window so that effects of catalyst poisoning would not impact the data presented.

3.4. *Improving CNT Adhesion to Polysilicon*

Integrating VMD platforms with cathodes that can provide high current density and long lifetime is a practical requirement for the industrial viability of packaged CNT field emission vacuum microelectronic devices (CNT FE-VMDs). In the previous sections, better control over CNT length and CNT forest morphology may be achieved through improved understanding of CNT growth kinetics on poly-Si, which is important

in precisely controlling the CNT-anode gap distance, for example. However, mechanisms of device failure must also be studied to improve device performance and lifetime. There have been numerous studies[70-72] on the failure mechanisms of standalone CNT field emitters that have identified several possible causes of failure. Examples include fracturing of the CNT tips during operation due to oxidative ablation of the CNTs caused by local resistive heating (*i.e.* thermo-mechanically activated fracture)[71, 73], degradation due to ion irradiation/bombardment[74, 75], and extraction of the CNT from the substrate due to either electrodynamic forces or increased resistive heating at the substrate-CNT interface[71, 72]. In the case of CNT emitters grown on MEMS polysilicon-based substrates, poor adhesion between the CNT emitter and its substrate is the primary limiting factor for overall device lifetime, although this can be mitigated to some extent by offsetting the gate laterally[76]. A loss of adhesion between the emitter and the substrate renders the emitter electrically inactive and could lead to catastrophic device failure if the emitter bridges electrically isolated components such as the cathode and the extraction grid. A common method to improve adhesion of thin films is to use layer of a refractory metal to improve adhesion between the substrate and the film. Because CNTs nucleate from a thin film catalyst, the integration of an adhesion layer between the polysilicon substrate and catalyst was investigated to improve adhesion of the CNT film, as this configuration most closely approximates CNTs grown on MEMS devices. While many groups have explored adhesion layers for CNT films on crystalline silicon and metallic substrates[77-79], to our knowledge this is the first investigation of CNT growth with metallic adhesion layers on polysilicon substrates. Titanium and molybdenum adhesion layers, or interlayers, were specifically chosen based on the best

literature results on crystalline silicon. They were compared to a reference sample without an adhesion layer. The titanium interlayer produced the best adhesion compared to the reference and the molybdenum interlayer samples (Figure 9).

The reflectance for the as-prepared films and the average reflectance after each subsequent tape pull were directly compared to the other interlayer samples by measuring against a control sample of a metal interlayer without a CNT forest. The titanium interlayer samples required 2.5 times more adhesion tests to reach saturation when compared to the reference sample, whereas the molybdenum showed only a small improvement of 1.3 times more than the reference sample. It was also seen throughout all the samples tested that the titanium interlayer samples had a final reflectance saturation point of approximately 35%, whereas the reference and molybdenum samples averaged approximately 40%. This could indicate that more CNT emitters remain permanently adhered and have an adherence strength larger than the removal force of the tape. This data indicates that using a titanium interlayer for CNT emitter growth on MEMS structures can offer improved adhesion properties, which could correspond to improved device lifetime. Furthermore, additional interactions could exist at the interface between the CNT emitter and the polycrystalline substrate that could reduce contact resistance and improve field emission properties of the emitter, such as preventing the formation of an iron silicide, thus reducing resistive heating at the substrate-CNT interface during operation of the emitter. These interactions will be the subject of future research.

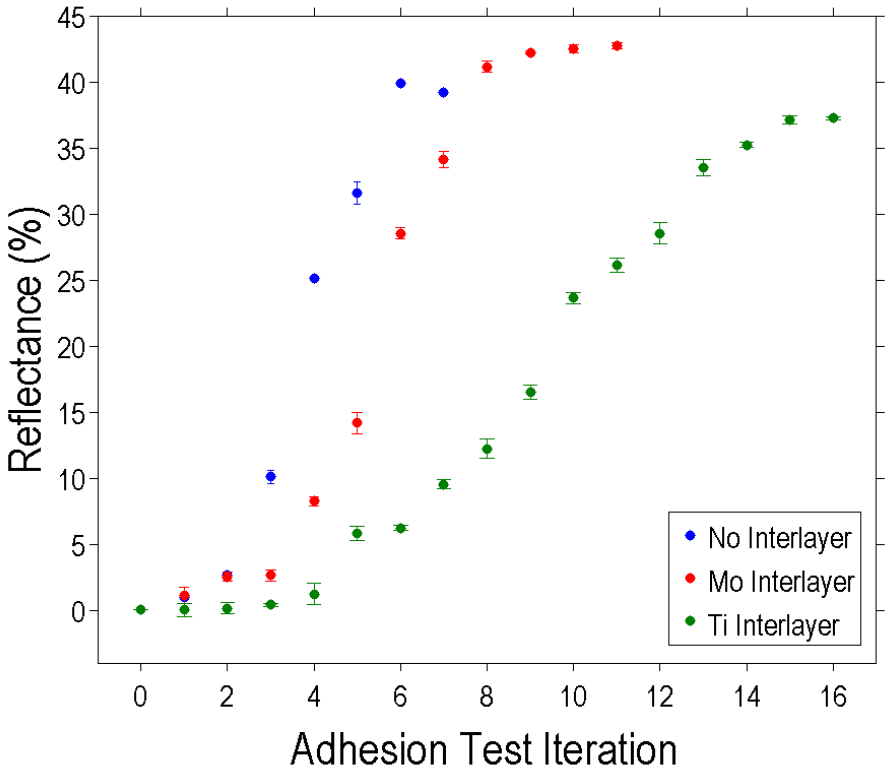

Figure 9: Average reflectance from the underlying substrate as measured by spectrophotometer for CNTs grown using various metallic interlayers. The error bars represent standard deviation. An adhesion improvement of approximately 1.3x was observed for Mo interlayers, and approximately 2.5x for Ti interlayers compared with the control sample of CNTs grown on Fe-coated poly-Si.

4. Conclusions

In this work, a method was validated for calculating reaction kinetics that may be applied to other systems. Growth of CNTs on polycrystalline silicon substrates has been studied to improve understanding of growth mechanics for applications in MEMS technology. The kinetics of CNT growth on polysilicon was elucidated using the model of Deal and Grove[41] to understand the activation energies and mechanisms for base-mediated growth using microwave PECVD. These results were compared to CNT growth on crystalline (100) silicon substrates, finding nucleation-stage activation energies that match literature values for bulk carbon diffusion into austenite catalyst nanoparticles.

Parabolic diffusion-limited growth was observed on each substrate, with activation energies for the diffusion-limited growth phase of 1.90 and 3.69 eV for growth on Si (100) and polysilicon, respectively, in the temperature range of 825 – 875 °C. A difference in overall diffusivity of carbon species through the growing CNT network was found, with values of 3.5×10^{-4} cm^2/s for growth on Si (100) and 7.9×10^{-5} cm^2/s for growth on polysilicon at 850 °C. In addition, deposition became diffusion limited earlier in the growth process using polysilicon substrates. Evidence was presented in favor of a growth mechanism involving surface diffusion of carbon species along the length of the growing CNTs from the gas phase to the catalyst at the base of the CNT forest, but some limited Knudsen diffusion may also occur. Possible reasons for this difference in diffusivity and the activation energy differences were explored through analysis of the catalyst nanoparticle dewetting process as well as subsequent changes in CNT tortuosity and alignment, as measured by WAXS. Finally, interlayer addition techniques were presented to improve CNT adhesion to polysilicon substrates for applications as cold cathode field emission sources for MEMS integration. Therefore, CNT forest integration into MEMS devices was improved through both an improvement in understanding of the growth kinetics, providing additional control over CNT film morphology, as well as an improvement in CNT adhesion to the substrate to extend device lifetime.

Acknowledgements

We are grateful to the Shared Materials Instrumentation Facility (SMiF) at Duke University for access to electron microscopy and Raman spectroscopy characterization tools. This material is based upon work supported by the National Science Foundation under Grant No. ECCS-1344745. The information, data, or work presented herein was funded in part by the Advanced Research Projects Agency-Energy (ARPA-E), U.S. Department of Energy, under Award Number DE-AR0000546. The views and opinions of authors expressed herein do not necessarily state or reflect those of the United States Government or any agency thereof. A portion of this work was performed under the auspices of the U.S. Department of Energy by Lawrence Livermore National Laboratory under Contract DE-AC52-07NA27344. X-ray characterization was performed at beamline 7.3.3[80] at the Advanced Light Source, which is supported by the Director, Office of Science, and Office of Basic Energy Sciences, of the U.S. Department of Energy under Contract No. DE-AC02-05CH11231.

References

[1] Spindt CA. A Thin‐Film Field‐Emission Cathode. Journal of Applied Physics. 1968;39(7):3504-5.
[2] Spindt CA, Holland CE, Rosengreen A, Brodie I. Field-emitter arrays for vacuum microelectronics. Electron Devices, IEEE Transactions on. 1991;38(10):2355-63.
[3] Brodi I. Physical considerations in vacuum microelectronics devices. Electron Devices, IEEE Transactions on. 1989;36(11):2641-4.
[4] Utsumi T. Vacuum microelectronics: what's new and exciting. Electron Devices, IEEE Transactions on. 1991;38(10):2276-83.
[5] Han J-W, Meyyappan M. Introducing the Vacuum Transistor: A Device Made of Nothing. IEEE Spectrum. 2014;51(7):30-5.
[6] Stoner BR, Glass JT. Nanoelectronics: Nothing is like a vacuum. Nat Nano. 2012;7(8):485-7.
[7] MEMSCAP. PolyMUMPs. [cited 2015; Available from: http://www.memscap.com/products/mumps/polymumps
[8] Natarajan S, Parker CB, Glass JT, Piascik JR, Gilchrist KH, Bower CA, et al. High voltage microelectromechanical systems platform for fully integrated, on-chip, vacuum electronic devices. Applied Physics Letters. 2008;92(22):224101.
[9] Gilchrist KH, Piascik JR, Stoner BR, Radauscher EJ, Amsden JJ, Parker CB, et al. Platform for integrated vacuum microelectronic circuits. Vacuum Electronics Conference, IEEE International; p. 155-6.
[10] Radauscher E, Keil A, Wells M, Amsden J, Piascik J, Parker C, et al. Chemical Ionization Mass Spectrometry Using Carbon Nanotube Field Emission Electron Sources. Journal of The American Society for Mass Spectrometry. 2015;26(11):1903-10.
[11] Baker RTK, Harris PS, Thomas RB, Waite RJ. Formation of filamentous carbon from iron, cobalt and chromium catalyzed decomposition of acetylene. Journal of Catalysis. 1973;30(1):86-95.
[12] Chhowalla M, Teo KBK, Ducati C, Rupesinghe NL, Amaratunga GAJ, Ferrari AC, et al. Growth process conditions of vertically aligned carbon nanotubes using plasma enhanced chemical vapor deposition. Journal of Applied Physics. 2001;90(10):5308-17.
[13] Hofmann S, Cantoro M, Kleinsorge B, Casiraghi C, Parvez A, Robertson J, et al. Effects of catalyst film thickness on plasma-enhanced carbon nanotube growth. Journal of Applied Physics. 2005;98(3):034308.
[14] Lee YT, Park J, Choi YS, Ryu H, Lee HJ. Temperature-Dependent Growth of Vertically Aligned Carbon Nanotubes in the Range 800−1100 °C. The Journal of Physical Chemistry B. 2002;106(31):7614-8.
[15] Kim K-E, Kim K-J, Jung WS, Bae SY, Park J, Choi J, et al. Investigation on the temperature-dependent growth rate of carbon nanotubes using chemical vapor deposition of ferrocene and acetylene. Chemical Physics Letters. 2005;401(4–6):459-64.

[16] Liu K, Jiang K, Feng C, Chen Z, Fan S. A growth mark method for studying growth mechanism of carbon nanotube arrays. Carbon. 2005;43(14):2850-6.
[17] Puretzky AA, Geohegan DB, Jesse S, Ivanov IN, Eres G. In situ measurements and modeling of carbon nanotube array growth kinetics during chemical vapor deposition. Applied Physics A. 2005;81(2):223-40.
[18] Vinten P, Lefebvre J, Finnie P. Kinetic critical temperature and optimized chemical vapor deposition growth of carbon nanotubes. Chemical Physics Letters. 2009;469(4–6):293-7.
[19] Zhu L, Xu J, Xiao F, Jiang H, Hess DW, Wong CP. The growth of carbon nanotube stacks in the kinetics-controlled regime. Carbon. 2007;45(2):344-8.
[20] Hofmann S, Ducati C, Robertson J, Kleinsorge B. Low-temperature growth of carbon nanotubes by plasma-enhanced chemical vapor deposition. Applied Physics Letters. 2003;83(1):135-7.
[21] Zhong, Iwasaki T, Robertson J, Kawarada H. Growth Kinetics of 0.5 cm Vertically Aligned Single-Walled Carbon Nanotubes. The Journal of Physical Chemistry B. 2007;111(8):1907-10.
[22] Noda S, Hasegawa K, Sugime H, Kakehi K, Zhang Z, Maruyama S, et al. Millimeter-thick single-walled carbon nanotube forests: Hidden role of catalyst support. Japanese journal of applied physics. 2007;46(5L):L399.
[23] Puretzky AA, Eres G, Rouleau CM, Ivanov IN, Geohegan DB. Real-time imaging of vertically aligned carbon nanotube array growth kinetics. Nanotechnology. 2008;19(5):055605.
[24] Zhu L, Hess DW, Wong C-P. Monitoring Carbon Nanotube Growth by Formation of Nanotube Stacks and Investigation of the Diffusion-Controlled Kinetics. The Journal of Physical Chemistry B. 2006;110(11):5445-9.
[25] Wirth CT, Zhang C, Zhong G, Hofmann S, Robertson J. Diffusion-and reaction-limited growth of carbon nanotube forests. ACS nano. 2009;3(11):3560-6.
[26] Louchev OA. Transport-kinetical phenomena in nanotube growth. Journal of Crystal Growth. 2002;237–239, Part 1:65-9.
[27] Louchev OA, Laude T, Sato Y, Kanda H. Diffusion-controlled kinetics of carbon nanotube forest growth by chemical vapor deposition. The Journal of Chemical Physics. 2003;118(16):7622-34.
[28] Wang L, Chen T, Feng T, Chen Y, Que W, Lin L, et al. Effect of sputtered Cu film's diffusion barrier on the growth and field emission properties of carbon nanotubes by chemical vapor deposition. Applied Physics A. 2007;90(4):701-4.
[29] Sharma H, Shukla AK, Vankar VD. Effect of titanium interlayer on the microstructure and electron emission characteristics of multiwalled carbon nanotubes. Journal of Applied Physics. 2011;110(3):033726.
[30] García-Céspedes J, Thomasson S, Teo KBK, Kinloch IA, Milne WI, Pascual E, et al. Efficient diffusion barrier layers for the catalytic growth of carbon nanotubes on copper substrates. Carbon. 2009;47(3):613-21.
[31] Stoner BR, Raut AS, Brown B, Parker CB, Glass JT. Graphenated Carbon Nanotubes for Enhanced Electrochemical Double Layer Capacitor Performance. Applied Physics Letters. 2011;99(18):183104.

[32] Parker CB, Raut AS, Brown B, Stoner BR, Glass JT. Three-Dimensional Arrays of Graphenated Carbon Nanotubes. Journal of Materials Research. 2012;27(07):1046-53.
[33] Ubnoske SM, Raut AS, Brown B, Parker CB, Stoner BR, Glass JT. Perspectives on the Growth of High Edge Density Carbon Nanostructures: Transitions from Vertically Oriented Graphene Nanosheets to Graphenated Carbon Nanotubes. J Phys Chem C. 2014;118(29):16126-32.
[34] Ubnoske SM, Raut AS, Parker CB, Glass JT, Stoner BR. Role of Nanocrystalline Domain Size on the Electrochemical Double-Layer Capacitance of High Edge Density Carbon Nanostructures. MRS Commun. 2015;5(02):285-90.
[35] Ubnoske SM, Peng Q, Meshot ER, Parker CB, Glass JT. Protocol for High-Sensitivity Surface Area Measurements of Nanostructured Films Enabled by Atomic Layer Deposition of TiO2. The Journal of Physical Chemistry C. 2015;119(46):26119-27.
[36] Brown B, Parker CB, Stoner BR, Glass JT. Growth of vertically aligned bamboo-like carbon nanotubes from ammonia/methane precursors using a platinum catalyst. Carbon. 2011;49(1):266-74.
[37] Futaba DN, Hata K, Yamada T, Hiraoka T, Hayamizu Y, Kakudate Y, et al. Shape-Engineerable and Highly Densely Packed Single-Walled Carbon Nanotubes and their Application as Super-Capacitor Electrodes. Nat Mater. 2006;5(12):987-94.
[38] ASTM D3359-09e2. Standard Test Methods for Measuring Adhesion by Tape Test. West Conshohocken, PA 2009.
[39] Lee SW, Kim KK, Cui Y, Lim SC, Cho YW, Kim SM, et al. Adhesion test of carbon nanotube film coated onto transparent conducting substrates. Nano. 2010;5(03):133-8.
[40] Fick A. V. On liquid diffusion. Philosophical Magazine Series 4. 1855;10(63):30-9.
[41] Deal BE, Grove AS. General Relationship for the Thermal Oxidation of Silicon. Journal of Applied Physics. 1965;36(12):3770-8.
[42] Cui H. Nucleation and Growth of Nanoscaled One-Dimentional Materials. University of North Carolina at Chapel Hill, Ph.D. Dissertation, 2001.
[43] Baker RTL, Barber MA. In: Walker PL, Thrower PA, eds. Chemical Physics and Carbon. New York: Dekker 1978.
[44] Geohegan DB, Puretzky AA, Ivanov IN, Jesse S, Eres G, Howe JY. In Situ Growth Rate Measurements and Length Control During Chemical Vapor Deposition of Vertically Aligned Multiwall Carbon Nanotubes. Applied Physics Letters. 2003;83(9):1851-3.
[45] Stadermann M, Sherlock SP, In J-B, Fornasiero F, Park HG, Artyukhin AB, et al. Mechanism and Kinetics of Growth Termination in Controlled Chemical Vapor Deposition Growth of Multiwall Carbon Nanotube Arrays. Nano Letters. 2009;9(2):738-44.
[46] Bedewy M, Meshot ER, Guo H, Verploegen EA, Lu W, Hart AJ. Collective Mechanism for the Evolution and Self-Termination of Vertically Aligned Carbon Nanotube Growth. The Journal of Physical Chemistry C. 2009;113(48):20576-82.

[47] Holstein WL. The Roles of Ordinary and Soret Diffusion in the Metal-Catalyzed Formation of Filamentous Carbon. Journal of Catalysis. 1995;152(1):42-51.
[48] Askeland DR. The Science and Engineering of Materials. Second Edition ed. Boston: PWS-KINT Publishing Company; 1989.
[49] Pathria RK. Statistical Mechanics. Second Edition ed. Oxford: Butterworth-Heinemann; 1996.
[50] Youngquist GR. Symposium on Flow through Porous Media: Diffusion and Flow of Gases in Porous Solids. Industrial & Engineering Chemistry. 1970;62(8):52-63.
[51] Scott DS, Dullien FAL. Diffusion of ideal gases in capillaries and porous solids. AIChE Journal. 1962;8(1):113-7.
[52] Hines AL, Maddox RN. Mass Transfer: Fundamentals and Applications. Englewood Cliffs, NJ: Prentice Hall; 1985.
[53] Cui H, Zhou O, Stoner BR. Deposition of aligned bamboo-like carbon nanotubes via microwave plasma enhanced chemical vapor deposition. Journal of Applied Physics. 2000;88(10):6072-4.
[54] Rostrup-Nielsen J, Trimm DL. Mechanisms of carbon formation on nickel-containing catalysts. Journal of Catalysis. 1977;48(1):155-65.
[55] Baker RTK, Chludzinski Jr JJ, Lund CRF. Further studies of the formation of filamentous carbon from the interaction of supported iron particles with acetylene. Carbon. 1987;25(2):295-303.
[56] Tuinstra F, Koenig JL. Raman Spectrum of Graphite. J Chem Phys. 1970;53(3):1126-30.
[57] Matthews MJ, Pimenta MA, Dresselhaus G, Dresselhaus MS, Endo M. Origin of dispersive effects of the Raman *D* band in carbon materials. Physical Review B. 1999;59(10):R6585-R8.
[58] Lee YH, Kim SG, Tománek D. Catalytic Growth of Single-Wall Carbon Nanotubes: An \textit{Ab Initio} Study. Physical Review Letters. 1997;78(12):2393-6.
[59] Henry PA, Raut AS, Ubnoske SM, Parker CB, Glass JT. Enhanced electron transfer kinetics through hybrid graphene-carbon nanotube films. Electrochemistry Communications. 2014;48(0):103-6.
[60] Choi YC, Shin YM, Lee YH, Lee BS, Park G-S, Choi WB, et al. Controlling the diameter, growth rate, and density of vertically aligned carbon nanotubes synthesized by microwave plasma-enhanced chemical vapor deposition. Applied Physics Letters. 2000;76(17):2367-9.
[61] Ren ZF, Huang ZP, Xu JW, Wang JH, Bush P, Siegal MP, et al. Synthesis of Large Arrays of Well-Aligned Carbon Nanotubes on Glass. Science. 1998;282(5391):1105-7.
[62] Choi H, Gong J, Lim Y, Im KH, Jeon M. Effects of the electrical conductivity and orientation of silicon substrate on the synthesis of multi-walled carbon nanotubes by thermal chemical vapor deposition. Nanoscale Research Letters. 2013;8(1):110.
[63] Huang Z, Wang D, Wen J, Sennett M, Gibson H, Ren Z. Effect of nickel, iron and cobalt on growth of aligned carbon nanotubes. Applied Physics A. 2002;74(3):387-91.

[64] Bower C, Zhou O, Zhu W, Werder DJ, Jin S. Nucleation and growth of carbon nanotubes by microwave plasma chemical vapor deposition. Applied Physics Letters. 2000;77(17):2767-9.
[65] Bedewy M, Meshot ER, Hart AJ. Diameter-dependent kinetics of activation and deactivation in carbon nanotube population growth. Carbon. 2012;50(14):5106-16.
[66] Bedewy M, Hart AJ. Mechanical coupling limits the density and quality of self-organized carbon nanotube growth. Nanoscale. 2013;5(7):2928-37.
[67] Bedewy M, Meshot ER, Reinker MJ, Hart AJ. Population Growth Dynamics of Carbon Nanotubes. ACS Nano. 2011;5(11):8974-89.
[68] Hermans PH. Contribution to the physics of cellulose fibres. 1946.
[69] Meshot ER, Bedewy M, Lyons KM, Woll AR, Juggernauth KA, Tawfick S, et al. Measuring the Lengthening Kinetics of Aligned Nanostructures by Spatiotemporal Correlation of Height and Orientation. Nanoscale. 2010;2(6):896-900.
[70] Williams LT, Kumsomboone VS, Ready WJ, Walker MLR. Lifetime and Failure Mechanisms of an Arrayed Carbon Nanotube Field Emission Cathode. Electron Devices, IEEE Transactions on. 2010;57(11):3163-8.
[71] Bonard J-M, Klinke C, Dean KA, Coll BF. Degradation and failure of carbon nanotube field emitters. Physical Review B. 2003;67(11):115406.
[72] Mahapatra DR, Sinha N, Melnik R. Degradation and Failure of Field Emitting Carbon Nanotube Arrays. Journal of nanoscience and nanotechnology. 2011;11(5):3911-5.
[73] Collins P, Avouris P. Multishell conduction in multiwalled carbon nanotubes. Applied Physics A. 2002;74(3):329-32.
[74] Deng J-H, Hou X-G, Cheng L, Wang F-J, Yu B, Li G-Z, et al. Irradiation Damage Determined Field Emission of Ion Irradiated Carbon Nanotubes. ACS applied materials & interfaces. 2014;6(7):5137-43.
[75] Bocharov GS, Eletskii AV. Degradation of a carbon nanotube-based field-emission cathode during ion sputtering. Technical Physics. 2012;57(7):1008-12.
[76] Sanborn G, Turano S, Collins P, Ready WJ. A thin film triode type carbon nanotube field emission cathode. Applied Physics A. 2013;110(1):99-104.
[77] Lahiri I, Choi W. Interface control: A modified rooting technique for enhancing field emission from multiwall carbon nanotube based bulk emitters. Acta Materialia. 2011;59(14):5411-21.
[78] Ominami Y, Ngo Q, Suzuki M, Austin AJ, Yang CY, Cassell AM, et al. Interface characteristics of vertically aligned carbon nanofibers for interconnect applications. Applied physics letters. 2006;89(26):263114.
[79] Lim SC, Choi HK, Jeong HJ, Song YI, Kim GY, Jung KT, et al. A strategy for forming robust adhesion with the substrate in a carbon-nanotube field-emission array. Carbon. 2006;44(13):2809-15.
[80] Alexander H, Wim B, James G, Eric S, Eliot G, Rick K, et al. A SAXS/WAXS/GISAXS Beamline with Multilayer Monochromator. Journal of Physics: Conference Series. 2010;247(1):012007.